Journal of Research and Applications in Mechanical Engineering
ISSN: 2229-2152 (Print); 2697-424x (Online)
(2025) Vol. 13, No. 1, Paper No. JRAME-25-13-011
[DOI: 10.14456/jrame.2025.11]

Research Article

Comparative Performance of Meta-Heuristic Algorithms for Low-Speed Wind Turbine Blade Structural Optimization

N. Sabangban
P. Suwunnasopha
K. Phuekpan
N. Phanwong
S. Bureerat
N. Pholdee
N. Panagant*
Sustainable and Infrastructure Research and Development Center, Department of Mechanical Engineering, Faculty of Engineering, Khon Kaen University, Khon Kaen 40002, Thailand

Received 4 April 2024
Revised 24 July 2024
Accepted 31 July 2024

Abstract:
The comparative assessment of recent Metaheuristics (MHs) optimization techniques was conducted within the context of low-speed wind turbine (LS-WT) blade design, with a focus on simultaneously addressing aerodynamic and structural considerations. The study encompasses two LS-WT design problems: the first aims to minimize wind turbine (WT) mass, while the second employs a weighted sum technique to simultaneously minimize WT mass and maximize turbine power. A comparative study on the performance of several recent MHs on the LS-WT problems has been conducted. The optimal design of the WT in the second problem exhibits greater dimensions compared to the shape in the first problem. The WT mass in the second problem is approximately 21 percent higher than in the first problem, reflecting the higher power output achieved in the second problem is more than 5.7 percent compared to the first problem. Statistical analysis of fitness values revealed that L-SHADE exhibited superior performance in terms of both average fitness and standard deviation compared to other algorithms.

Keywords: *Metaheuristic, Wind turbine, Low speed wind turbine, Optimization*

1. Introduction

Optimization techniques have been instrumental in tackling real-world problems, spanning a wide array of complexities and challenging functions. In general, MHs are highly popular for solving optimization problems because they are based on randomization and gradient-based free. The advantages mentioned above also prevent the occurrence of local traps in the search domain and enhance the diversity of results in optimization processes. Hence, researchers are continuously developing new algorithms to effectively address and overcome a myriad of challenges posed by various problems. In engineering problems such as WT blade design [1-5], the variables encompass both the geometric shape and structural components, demonstrating interdependence. The optimal outcomes indicate that the WT blade has achieved the highest turbine power generation while simultaneously ensuring structural stability.

In the domain of optimization processes, MHs are utilized to identify optimal design variables encapsulated within vectors. Subsequently, these design variables are evaluated to ascertain the objective function, the objective value, constraints, and optimal design variables were selected in the selection process. Then, the optimizer initiates the reproduction process by generating new values for the design variables randomly around the optimal solution, referred to as offspring. It is noteworthy that the strategy employed by each optimizer influences the generation of different offspring, thereby impacting the performance of each algorithm. Indeed, several classical MHs, including Genetic

* Corresponding author: N. Panagant
E-mail address: natepa@kku.ac.th

Algorithm (GA) [6-9], Artificial Bee Colony Algorithm (ABC) [10], and Particle Swarm Optimizer (PSO) [11, 12] have been extensively studied. These algorithms encounter challenges across a diverse range of benchmark functions. However, in recent times, enhanced MH algorithms have emerged to address these challenges. Examples include Success-History based Adaptive Differential Evolution (SHADE) [13, 14], Success-History based Adaptive Differential Evolution with Linear population size reduction (L-SHADE) [15, 16], Chinese Pangolin Optimizer (CPO) [17], Electric Eel Foraging Optimization (EEFO) [18], Marine Predators Algorithm (MPA) [19] and, Quadratic Interpolation Optimization (QIO) [20]. These algorithms are tailored to address the intricacies presented by a wide array of benchmark functions. Moreover, the development of MHs can solve real-world problems, including the design WT blade.

Typically, WT blade designs commence with conceptualization, wherein design variables such as twisted angle (β) [6, 21], chord length (c) [6, 21], and airfoil type [7, 22] are considered. The primary objective at this stage is to identify the optimum shape that yields the highest power output [6, 21-26], which studied in conceptual design phase. They are calculated the power by the Blade Element Momentum (BEM) method. Subsequently, during the preliminary design phase, structural considerations come into play, the objective is to minimize the WT blade mass [4, 27-30]. This involves determining the topology of the WT blade [4, 11, 30], as well as specifying parameters such as thickness, orientation, and the number of layers of carbon fiber in skins, spars, and ribs [27-29, 31, 32]. The structural design variables are meshed and evaluated in Finite Element Analysis (FEA) to identify the structural constraints. Parameters such as blade tip deflection (δ) [4, 31], Tsai-Hill failure criterion (TH) [28] and buckling factor (Bf) [4, 29] are identified as key constraints in the optimization of WT blade structure.

In the literature, the simultaneous design between aerodynamics and structure has limitation to study [30, 33, 34]. Furthermore, a majority of these investigations predominantly focus on medium wind speeds, typically around 15 m/s. To address the notable gaps in the existing research, this study investigated the concurrent design of aerodynamics and structure for LS-WT blade. Additionally, the study aimed to identify the most effective recent MH algorithm for further enhancement.

In this research, four recent single objective meta-heuristics (SOMH) algorithms, namely L-SHADE, EEFO, MPA, and QIO were evaluated, in the context of LS-WT design. This problem encompasses both aerodynamics and structural considerations simultaneously. There are 2 problem statements presented in LS-WT, which present the various of design configuration. First, the objective of the optimization is to minimize the mass of the wind turbine (WT) blade. Second, the objective is focused on mass and power by weighted sum technique. To ensure the feasibility of the design, constraints related to WT blade deflection, buckling factor, Tsai-Hill failure, and turbine power are incorporated into the optimization process. The problem definitions are shown in this research. Their contributions in this study are presented as follows:

1) Simultaneous aerodynamics and structure design was evaluated by single-objective optimization, which includes 2 problem designs.
2) The design of the WT blade is being rigorously examined under low-speed conditions, specifically at a wind speed of 5 m/s.
3) Comparing and assessing the effectiveness of recent meta-heuristics is essential for their ongoing development.

2. Methodology

In general, WT blade design takes into account both aerodynamics and structural integrity. The aerodynamics affect the torque, while the structural integrity influences the strength of the WT structure. Therefore, an optimal design must consider both the WT power output and the blade mass.

2.1 Aerodynamic analysis in Blade Element Momentum (BEM)

For aerodynamic analysis, the BEM theory is a widely used method for analyzing the performance and aerodynamics of wind turbine blades [35-37]. It combines blade element theory as shown in Equation 1 and Equation 2, which divides the blade into several small sections (blade elements) and calculates the aerodynamic forces (lift and drag) acting on each section based on local flow conditions with momentum theory, which considers the conservation of linear and angular momentum in the airflow through the wind turbine rotor in Equation 3 and Equation 4.

$$L = \frac{1}{2}\rho v^2 c_l c \tag{1}$$

$$D = \frac{1}{2}\rho v^2 c_d c \tag{2}$$

Where ρ is the air density, v is the relative wind speed, c_l and c_d are lift and drag coefficients, and c is the chord length.

$$T = \dot{m}(v_1 - v_2) \tag{3}$$

$$P = \frac{\dot{m}}{2}(v_1^2 - v_2^2) \tag{4}$$

where T is thrust, P is turbine power, $\dot{m}$ is mass flow rate, v_1 and v_2 are upstream and downstream wind speed respectively. BEM theory integrates these local aerodynamic forces with the overall momentum changes in the airflow, using iterative calculations to ensure consistency between the blade element forces and the momentum changes. This approach provides insights into the performance characteristics of the wind turbine, such as power output, thrust, and efficiency as shown in Equation 5, making it essential for the design optimization of wind turbine blades.

$$P = \sum(L_i \sin\emptyset - D_i \cos\emptyset)\tau_i\, \omega \tag{5}$$

Where $\emptyset$ is the inflow angle, τ_i is the radial position of the element, and ω is the angular velocity. More details of the BEM algorithm can be found in the AeroDyn theory manual [38]. Despite its simplified assumptions, such as uniform inflow and steady-state conditions, the BEM theory offers a balance between computational efficiency and the level of details needed for practical wind turbine design and analysis, with corrections like tip loss factors and dynamic stall models often applied to enhance its accuracy.

2.2 Structural Analysis

2.2.1 Static Finite Element Analysis

In this study, the quadratic shell elements were applied in FEA for calculating structural displacements, stresses, and buckling factors while the Tsai-Hill criterion is used for composite material failure prediction. The structural finite element analysis is based upon the principle of minimum potential energy. A linear displacement-based finite element approach is used. The structure is in an equilibrium state when its total potential energy is minimized leading to a system of linear equations.

$$[\boldsymbol{K}]\{\boldsymbol{r}\} = \{\boldsymbol{F}\} \tag{6}$$

where $[\boldsymbol{K}]$ is a global stiffness matrix, $\{\boldsymbol{r}\}$ is a nodal displacement vector, and $\{\boldsymbol{F}\}$ is the vector of applied loads. When dealing with prespecified boundary conditions, the system of linear equations must be partitioned and solved as:

$$\begin{bmatrix} \boldsymbol{K}_{aa} & \boldsymbol{K}_{ab} \\ \boldsymbol{K}_{ba} & \boldsymbol{K}_{bb} \end{bmatrix} \begin{Bmatrix} \boldsymbol{r}_a \\ \boldsymbol{r}_b \end{Bmatrix} = \begin{Bmatrix} \boldsymbol{F}_a \\ \boldsymbol{F}_b \end{Bmatrix} \tag{7}$$

$$\boldsymbol{r}_a = \boldsymbol{K}_{aa}^{-1}(\boldsymbol{F}_a - \boldsymbol{r}_b) \tag{8}$$

Here, $\boldsymbol{r}_a$ is the vector of unknown nodal displacements, $\boldsymbol{r}_b$is the vector of predefined displacements, $\boldsymbol{F}_a$is the vector of known applied loads, and $\boldsymbol{F}_b$is the vector of unknown reactions. Having solved for $\boldsymbol{r}_a$, the stress recovery on element *e* is carried out by using the relation

$$\{\boldsymbol{\sigma}^e\} = [\boldsymbol{D}][\boldsymbol{B}]\{\boldsymbol{r}^e\} \tag{9}$$

where $\{\boldsymbol{\sigma}^e\}$ is the vector of stresses at a point on shell element *e*, $[\boldsymbol{D}]$ is an elasticity matrix, $[\boldsymbol{B}]$ is a strain matrix, and $\{\boldsymbol{r}^e\}$ is the vector of element nodal displacements.

2.2.2 Tsai-Hill Failure Criterion

Once the nodal stresses are calculated, the Tsai-Hill failure criterion (TH) is used to predict failure in composite materials under complex loading conditions. It extends the von Mises yield criterion to anisotropic materials, like fiber-reinforced composites [39, 40]. The formulation of the TH involves a combination of stress components expressed as follows:

$$TH = \left(\frac{\sigma_1^2}{\sigma_{a,1}^2}\right) + \left(\frac{\sigma_2^2}{\sigma_{a,2}^2}\right) + \left(\frac{\tau_{12}^2}{\tau_{a,12}^2}\right) - \left(\frac{\sigma_1\sigma_2}{\sigma_{a,1}^2}\right) \tag{10}$$

where σ_1, σ_2, and τ_{12} represent the longitudinal, transverse, and shear stresses occurring in the composite layers. The variable of $\sigma_{a,1}$, $\sigma_{a,2}$, and $\tau_{a,12}$ are the corresponding allowable stress in those directions respectively. If the TH inequality is satisfied (≤ 1), the material is considered safe under the applied stresses. If it exceeds 1, failure is predicted due to stress levels surpassing the material's capacity. This criterion is pivotal for evaluating and designing reliable composite structures.

2.2.3 Buckling Analysis

Buckling analysis here is bifurcation buckling used to predict structural instability subject to axial or in-plane loadings. When the structure is initially applied by external loads, a static finite element analysis [41, 42] is conducted while the applied stresses are obtained. The work done by the in-plane stresses due to bending of the shells is then calculated. Applying the minimum potential energy state leads to an eigenvalue problem.

$$[\boldsymbol{K} + \lambda\boldsymbol{G}]\boldsymbol{r} = 0 \tag{11}$$

where λ is the eigenvalue that represents to the ratio of critical to applied loads, $\boldsymbol{G}$ is the geometrical stiffness matrix due to prestress, and $\boldsymbol{r}$ is a buckling eigenvector. Solving this eigenvalue problem provides the critical buckling load, corresponding to the smallest eigenvalue λ, which is considered as one of the design constraints.

2.3 Problem Definition

The optimization of the LS-WT blade design problem was approached through single-objective optimization. The problem definition in this research is outlined as follows:

2.3.1 Optimization of LS-WT Blade Design for Mass Minimization

The first design problem is LS-WT blade constitutes a single objective and four constraints. The optimization problem is expressed through mathematical equations from Equation 12 - 16 as follows:

Objective: $f(x) = min(WT_{mass}); x = \begin{Bmatrix} x_{structure} \\ x_{shape} \end{Bmatrix}$ (12)

Subject to: $g_1(x) = \frac{|\delta_{max}|}{\delta_a} - 1 \leq 0$ (13)

$g_2(x) = 1 - Bf_{min} \leq 0$ (14)

$g_3(x) = TH_{min} - 1 \leq 0$ (15)

$g_4(x) = P_a - P_{WT} \leq 0$ (16)

Where δ_a represents the allowable displacement of the WT blade, which is set to 0.05 m, equivalent to 5% of the blade span. The P_a denotes the allowable WT power, must be higher than 90 kW.

In this context, the variable x represents an array containing the design variables, encompassing both the structural and aerodynamic parameters of the WT blade. The symbols WT_{mass}, δ_{max}, Bf_{min}, TH_{min}, and P_{WT} denote the mass of the WT blade, maximum blade deflection, minimum buckling factors occurring in the WT blade, minimum Tsai-Hill failure criteria, allowable WT power and the power generated by the WT, respectively.

For the evaluation process, the shape design variables (x_{41} to x_{48}) are generated the distribution of chord and twist angle by Piecewise Cubic Hermite Interpolating Polynomial (PCHIP). The shape distribution is used to compute the P_{WT} using BEM theory. In the fourth constraint $g_4(x)$, the minimum WT power output must ≥ 90 kW at low wind speed (5 m/s). The BEM involves obtaining the aerodynamic loads in the horizontal (Fx) and vertical (Fz) directions. Subsequently, the structure (x_1 to x_{40}) and shape design variables are integrated into a FEA model. The model consisted of 1,490 nodes and 1,836 elements, with shell elements utilized as the element type as displayed in Fig. 1a. The boundary conditions, comprising forces in the x-direction (Fx), forces in the z-direction (Fz) and fixed support, are illustrated in Fig. 1b. It should be noted that the forces Fx and Fz are derived from BEM and exhibit variations depending on the WT shape. Three constants, denoted as $g_1(x)$, $g_2(x)$, and $g_3(x)$, were evaluated using Finite Element Analysis (FEA) in NASTRAN software. Additionally, the δ_a is assigned as 5% of the blade span. Then, the results of function including $f(x)$, $g_1(x)$, $g_2(x)$, $g_3(x)$, and $g_4(x)$ are sent to algorithms. The algorithm selects the best solution from the LS-WT function, updates its strategies, and initiates reproduction again until termination criteria are met.

2.3.2 Optimizing the Performance of LS-WT Blades for Minimizing Mass and Maximizing Power using the Weighted Sum Method.

In the second design problem, both WT mass (f_{mass}) and WT power (f_{power}) are considered as objective functions. The constraints are the same as the first problem except the WT power is instead assigned as the second objective of this problem. Both objectives are normalized before they are converted into a single objective with weighted sum technique [43-45]. The weight factors, decided by a designer, determine the tradeoff between objective functions. In this study, to simplify the LS-WT problem, the weight factors for f_{mass} and f_{power} were set equally because this research considers both objectives equally important. The problem is then transformed into a single objective optimization problem as described in Equation 17-21.

$$\text{Objective: } f(x) = w_1(f_{mass}) + w_2(f_{power});\ x = \begin{Bmatrix} x_{structure} \\ x_{shape} \end{Bmatrix} \tag{17}$$

$$f_{mass} = min(WT_{mass});\ f_{power} = max(WT_{power}) \tag{18}$$

$$\text{Subject to: } g_1(x) = \frac{|\delta_{max}|}{\delta_a} - 1 \leq 0 \tag{19}$$

$$g_2(x) = 1 - Bf_{min} \leq 0 \tag{20}$$

$$g_3(x) = TH_{min} - 1 \leq 0 \tag{21}$$

where w_1 and w_2 represent the weights assigned to each objective. In this study, WT mass and power output are assigned the same level of influence on the fitness [43]. Therefore, the weights values of w_1 and w_2 are each set to 0.5.

There are 48 design variables depicted in Table 1, representing the thicknesses and orientations of the upper skin, lower skin, ribs, and spars. In the Table 1, N is the maximum positive integer in spar thickness and N_{inc} is the increment value of spar thickness. The design variables, denoted as $x_{structure}$ and x_{shape} are explained as follow:

$$\boldsymbol{x}_{structure} = \{x_1, x_2, x_3, \ldots\ x_{40}\}$$
$$\boldsymbol{x}_{shape} = \{x_{41}, x_{42}, x_{43}, \ldots\ x_{48}\}$$

All structures in the WT blade were constructed by carbon fiber as shown in Table 2. The shape design variables, including chord and twist distributions, are generated using control points, as illustrated in Fig. 2. There are four design variables serving as control points for chord distribution and four design variables for twist angle distribution along the blade span. The constraint design variables for chord and twist angle are presented in Table 1. The PCHIP technique was utilized to interpolate and define the shape of the WT through an interpolation curve. Subsequently, 17 airfoils were substituted, and the chord length and twist angle of each blade section are adjusted according to the interpolation curve. This research begins by formulating design problems in LS-WT, considering both aerodynamics and structural integrity simultaneously. To simplify this problem, the characteristics of each airfoil were fixed in each section while the airfoil type on each blade section is fixed as shown in Table 3.

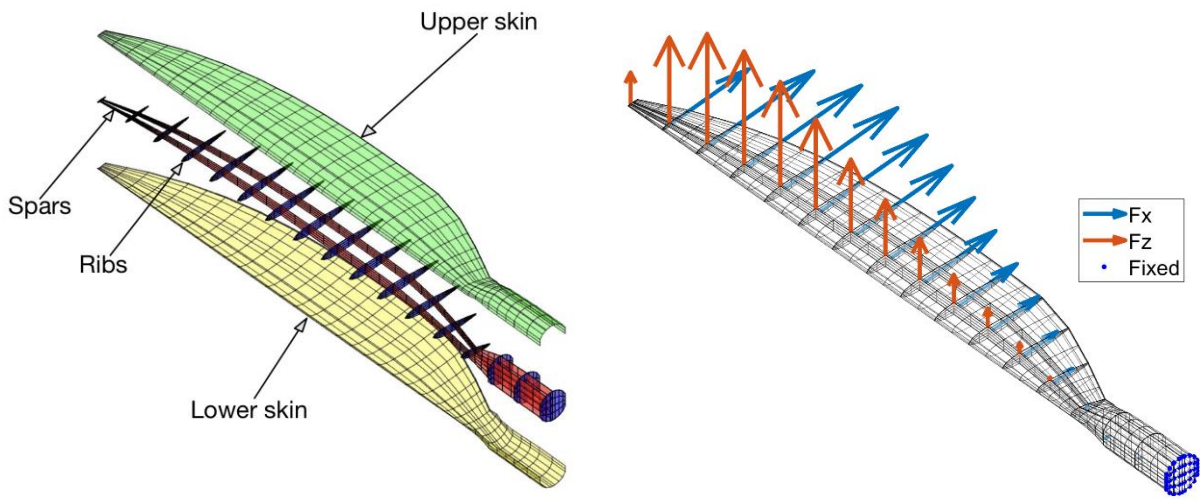

(a) (b)

Fig. 1. The FEA model (a) the components of WT blade and (b) FEA mesh, loadings, and fixed supports.

Table 1: Design variables.

Design Variables	Values (Units)	Descriptions
x_1 to x_5	{0.1, 0.2, 0.3, …, 5} (m)	Upper skin thickness Layer 1:5
x_6 to x_{10}	{0, 45, 90, 135} (deg)	Upper skin orientation Layer 1:5
x_{11} to x_{15}	{0.1, 0.2, 0.3, …, 5} (m)	Lower skin thickness Layer 1:5
x_{16} to x_{20}	{0, 45, 90, 135} (deg)	Lower skin orientation Layer 1:5
x_{21} to x_{25}	$\{1, 2, 3, \ldots, 20\} \times 10^{-3}$ (m)	Rib thickness Layer 1:5
x_{26} to x_{30}	{0, 45, 90, 135} (deg)	Rib orientation Layer 1:5
x_{31} to x_{35}	$\{1.5, 1.5 + N_{inc}, 1.5 + 2N_{inc}, \ldots, N\} \times 10^{-3}$(m) Where: $N = (x_{44}/1.5)$, and $N_{inc} = \frac{N-1.5}{20}$ (m)	Spar thickness Layer 1:5
x_{36} to x_{40}	{0, 45, 90, 135} (deg)	Spar orientation Layer 1:5
x_{41} to x_{44}	$0.3 \geq x_{41} \geq 0.7$ (m) $2 \geq x_{42} \geq 6$ (m) $0.6 \geq x_{43} \geq 1.5$ (m) $0.09 \geq x_{44} \geq 0.5$ (m)	Control points in the chord distribution
x_{45} to x_{48}	$8 \geq x_{45} \geq 17$ (deg) $2 \geq x_{46} \geq 6$ (m) $4 \geq x_{47} \geq 12$ (deg) $-0.25 \geq x_{48} \geq 1$(deg)	Control points in the twist distribution

Table 2: Material properties

Symbols	Descriptions	Values (Units)
E_{11}	Elastic modulus in *x*-direction	135 (GPa)
E_{22}	Elastic modulus in *y*-direction	10 (GPa)
G_{12}	Shear modulus in *xy*-direction	5 (GPa)
G_{13}	Shear modulus in *xz*-direction	5 (GPa)
G_{23}	Shear modulus in *yz*-direction	5 (GPa)
v	Poisson's ratio	0.3
ρ	Material density	1,600 (kg/m^3)
$\sigma^a_{t(1,1)}$	Allowable tensile stress in longitudinal direction	750 (MPa)
$\sigma^a_{t(2,2)}$	Allowable tensile stress in transverse direction	25 (MPa)
$\tau^a_{t(1,2)}$	Allowable tensile shear stress	35 (MPa)
$\sigma^a_{c(1,1)}$	Allowable compressive stress in longitudinal direction	600 (MPa)
$\sigma^a_{c(2,2)}$	Allowable compressive stress in transverse direction	125 (MPa)
$\tau^a_{c(1,2)}$	Allowable compressive shear stress	35 (MPa)
Sb_a	Allowable bonding stress	5 (MPa)

Table 3: Type and position of airfoil.

Airfoil sections	Position from the root (m)	Airfoil types	Airfoil sections	Position from the root (m)	Airfoil types	Airfoil sections	Position from the root (m)	Airfoil types
1	0	Cylinder	7	3.66	NACA0015	13	7.46	NACA0015
2	0.59	Cylinder	8	4.29	NACA0015	14	8.10	NACA0015
3	1.17	Cylinder	9	4.93	NACA0015	15	8.73	NACA0015
4	1.76	NACA0024	10	5.56	NACA0015	16	9.37	NACA0015
5	2.39	NACA0018	11	6.20	NACA0015	17	10.00	NACA0015
6	3.02	NACA0015	12	6.83	NACA0015			

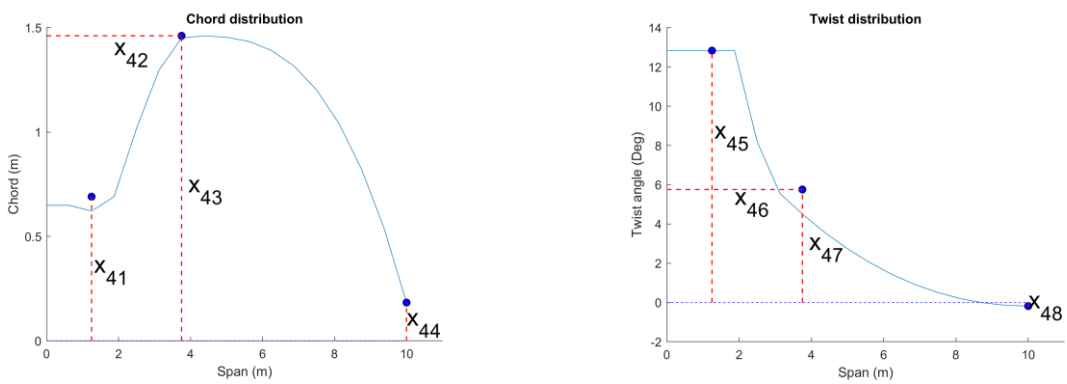

(a) (b)

Fig. 2. The distribution of control points in shape design variables (a) chord distribution and (b) twist angle distribution.

During the optimization process, the algorithms generate initial parameters and design variables, which are subsequently evaluated using the LS-WT function, as illustrated in Fig. 3. There are two problems that were executed separately during function evaluation. In function evaluation, the $\boldsymbol{x}_{shape}$ represents the generated dimensions of the WT blade, which are used to calculate the WT power and aerodynamic forces using BEM. Mesh generation is then applied to the WT shape. Subsequently, the $\boldsymbol{x}_{structure}$ variables, representing WT thickness and orientation of skin, ribs, and spars, are generated. The aerodynamic forces are transferred to the FEA model, where the constraints and objective functions are evaluated as output variables. These variables are then responsive to the optimization process, which updates the fitness, selection, and adaptive parameters for the next evaluation until the termination criteria are met.

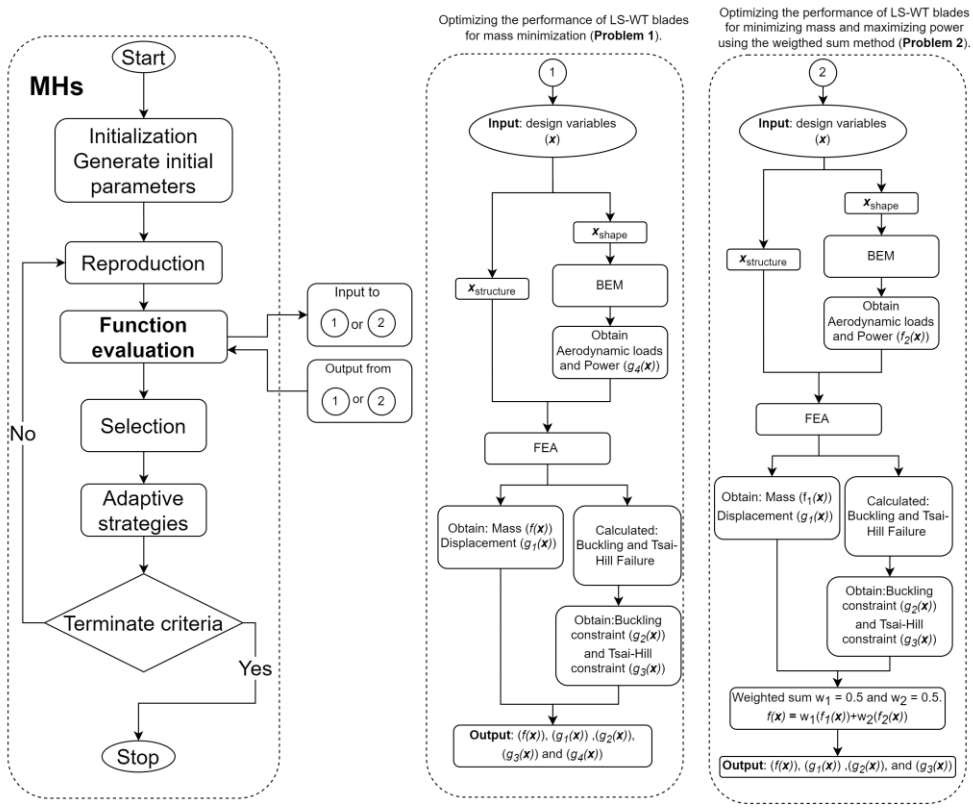

Fig. 3. The flowchart of MHs and LS-WT function

3. Numerical Experiment

In this study, four SOMHs, namely L-SHADE, EEFO, MPA, and QIO, were assessed for their performance in optimizing the LS-WT blade design function. The parameters for this optimization problem, including the maximum number of function evaluations (fe_{max}), the initial population size (n_p), and number of runs (n_r) were set to 10,000, 100, and 10 respectively. The parameter configurations for each algorithm are outlined as follows:

3.1. Improving the Search Performance of SHADE Using Linear Population Size Reduction (L-SHADE)

This algorithm was improved from Success-History Based Parameter Adaptation for Differential Evolution (SHADE) [13, 14] and Differential Evolution (DE) [46], utilizing parameters such as the scaling factor (SF) and crossover constant (CR) from DE. The parameters including the external archive memory (A), number of minimum population (NP_{min}), linearly related reducing population (NA_g), percent of best individuals in the population ($p\%$) are 5,4, and 14(NP_g) where NP_g is the number of current populations [15].

3.2. Electric Eel Foraging Optimization (EEFO)

The algorithm parameters include several equations, referencing factors such as the energy factor (E), scale of resting area ($Alpha$), scale of hunting area ($Beta$) and Curling factor (Eta) [18].

3.3. Marine Predators Algorithm (MPA)

The algorithm which used Eddy formation to update reproduction parameters. The parameters include Fish Aggregating Devices (FADs) and constant number in movement of prey (P) are 0.2 and 0.5 respectively [19].

3.4. Quadratic Interpolation Optimization (QIO)

The algorithm approximates the minimum point using a quadratic interpolation polynomial. It involves schematic exploration and exploitation parameters represented by three undetermined coefficients: $Alpha$, $Beta$, and $Delta$ [20].

4. Results and Discussions

In the results, two LS-WT problems with differing objectives and constraints are examined. The first problem seeks to minimize WT mass while ensuring that WT power remains above 90 kW. In contrast, the second problem employs a weighted sum technique to simultaneously optimize WT mass and WT power.

To identify the performance of the SOMHs, statistical results are obtained in LS-WT design problems. The average real fitness and standard deviation from 10 runs are performed the measure performance of algorithms. The results are presented in Table 4. It should be noted that all algorithms were subjected to 10,000 function evaluations for both Problem 1 and Problem 2. The best algorithm was then determined based on the mean objective value at the conclusion of these evaluations.

In the table, speed of algorithms is measured by mean fitness and Friedman's ranks while consistency is indicated with worst fitness and standard deviation (std). The best fitness found by all algorithms are also included in the paper. From the results, L-SHADE is obviously the best algorithm since it obtained the best results of all statistical indicators. In speed aspect, the mean fitness and Friedman's rank coincide in both problems. L-SHADE is obviously the best algorithm for both problems while SOMPA and SOEEFO are the runner-up and the third, respectively. For SOQIO, it is dominated in the first problem, but its mean fitness is on par with SOMPA in the second problem. L-SHADE is also the most consistent algorithm considered the best standard deviation and worst fitness. SOEEFO and SOMPA performed with a close consistent performance in the first problem, but SOEEFO is slightly better in the second problem. SOQIO is the worst algorithm in this study. Overall, L-SHADE outperformed all competitors and regarded as a winner on these WT optimization problems.

Table 4: Statistical results of real fitness

Problem	Statistics	L-SHADE	SOEEFO	SOMPA	SOQIO
Problem no.1	mean	**192.5753**	400.9392	353.235	468.269
	worst	**213.1412**	472.5427	414.7221	572.4131
	best	**180.0153**	352.2627	276.512	383.0829
	std	**9.976825**	35.19351	37.33781	67.15417
	rank	**1**	3.1	2.2	3.7
Problem no.2	mean	**0.044786**	0.056038	0.060272	0.060825
	worst	**0.045485**	0.059852	0.065739	0.067988
	best	**0.043917**	0.053935	0.055997	0.056054
	std	**0.000645**	0.001792	0.003071	0.003644
	rank	**1**	2.1	3.3	3.6
mean F-rank		**1**	2.6	2.75	3.65

In Table 5, the Wilcoxon signed-rank test is evaluated to ensure significant of different search performance. It is noteworthy that the output indicates significant evidence (p-value < 0.05) of a difference between the fitness. In the table, the best performer, L-SHADE is assigned as the reference algorithm. From the results, L-SHADE is significantly better than all other competitors in both problems.

Table 5: Wilcoxon Rank sign rank test and ranking of algorithms for WT Problems no.1 and no.2 (5% significant)

Problem	L-SHADE	SOEEFO	SOMPA	SOQIO
Problem no.1	1	3 (+)	2 (+)	4 (+)
Rank average	1	3	2	4
Problem no.2	1	2 (+)	3 (+)	4 (+)
Rank average	1	2	3	4
+/-/=	NA	**2**\0\0	**2**\0\0	**2**\0\0

The fitness history for all algorithms is presented in Fig. 4. In the first problem, initially, the fitness of SOMPA was better than that of the other algorithms until 1,000 function evaluations. However, beyond 2,000 function evaluations, L-SHADE performed with superior performance compared to the rest algorithms. It was observed that the final solutions obtained by L-SHADE exhibited significantly better fitness. At 4,000 function evaluations, the results of SOEEFO and SOMPA are approximately equivalent. By 8,000 function evaluations, both algorithms become trapped in local optima. For the second problem, SOMPA exhibits a similar trend as observed in the first problem, where it initially achieved the best fitness during the early evaluations. Subsequently, L-SHADE deviated from the others around 1,500 function evaluations and proceeded to outperform the rest of the algorithms. Notably, at 4,000 function evaluations, the fitness of SOEEFO is lower than that of SOMPA. However, all three algorithms SOEEFO, SOMPA, and SOQIO remain stuck in local optima, resulting in significantly worse final fitness compared to L-SHADE.

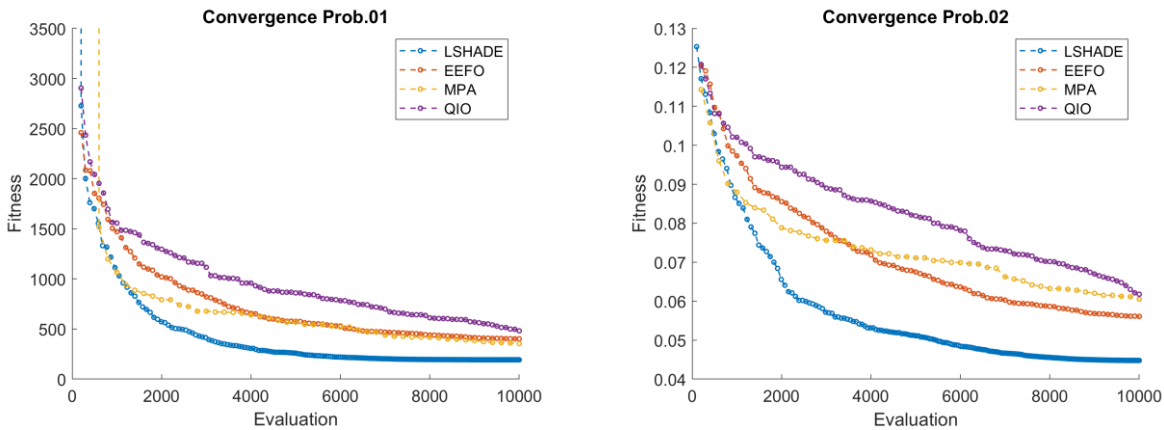

Fig. 4. Convergence fitness (a) the convergence of problem no.1 and (b) the convergence of problem no.2.

The findings from L-SHADE indicate that the optimal design shape in the first problem and the second problem is illustrated in Fig. 5. This outcome suggests a nuanced approach to design optimization; while the optimal design in the second problem focuses on enhancing WT power, the design in the first problem prioritizes minimizing WT mass within the specified power threshold. A noteworthy observation is that the optimal shape derived from the second problem tends to be larger, facilitating enhanced wind energy harnessing for efficient electricity production.

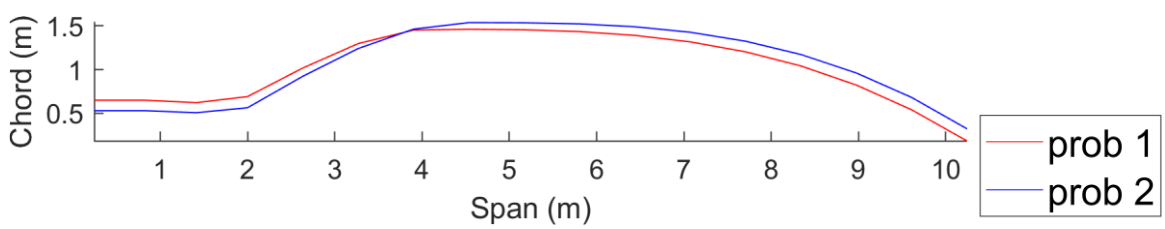

Fig. 5. The optimal shape in the first and the second WT design problem.

Fig. 6 presents the characteristics of 17 airfoil sections, showcasing the varying results in WT shapes. It's evident that the cylindrical airfoil shape in the first problem (Fig. 6a to Fig. 6c) exceeds that of the second problem. Specifically, from section 8 to section 17 (Fig. 6d to Fig. 6q), the airfoil of the second problem begins to exhibit a larger size compared to the first problem. Consequently, the difference in objectives has a significant effect on the aerodynamic shape of the WT blade.

Furthermore, Table 6 provides the design variables, objectives, and constraints of the best solutions obtained by L-SHADE. With power constraint in the first problem, the algorithm is sought for the smaller blade and lighter structure while avoiding constraint violation. This leads to lighter and smaller blade with power output very close to 90 kW as assigned in the constraint equation. In contrast, the optimal design from the second problem exhibits higher aerodynamic forces and power output, albeit at the expense of a heavier structure. This trade-off is reasonable,

considering that the second problem incorporates both WT mass and WT power output as objective functions, whereas only WT mass is considered in the first problem.

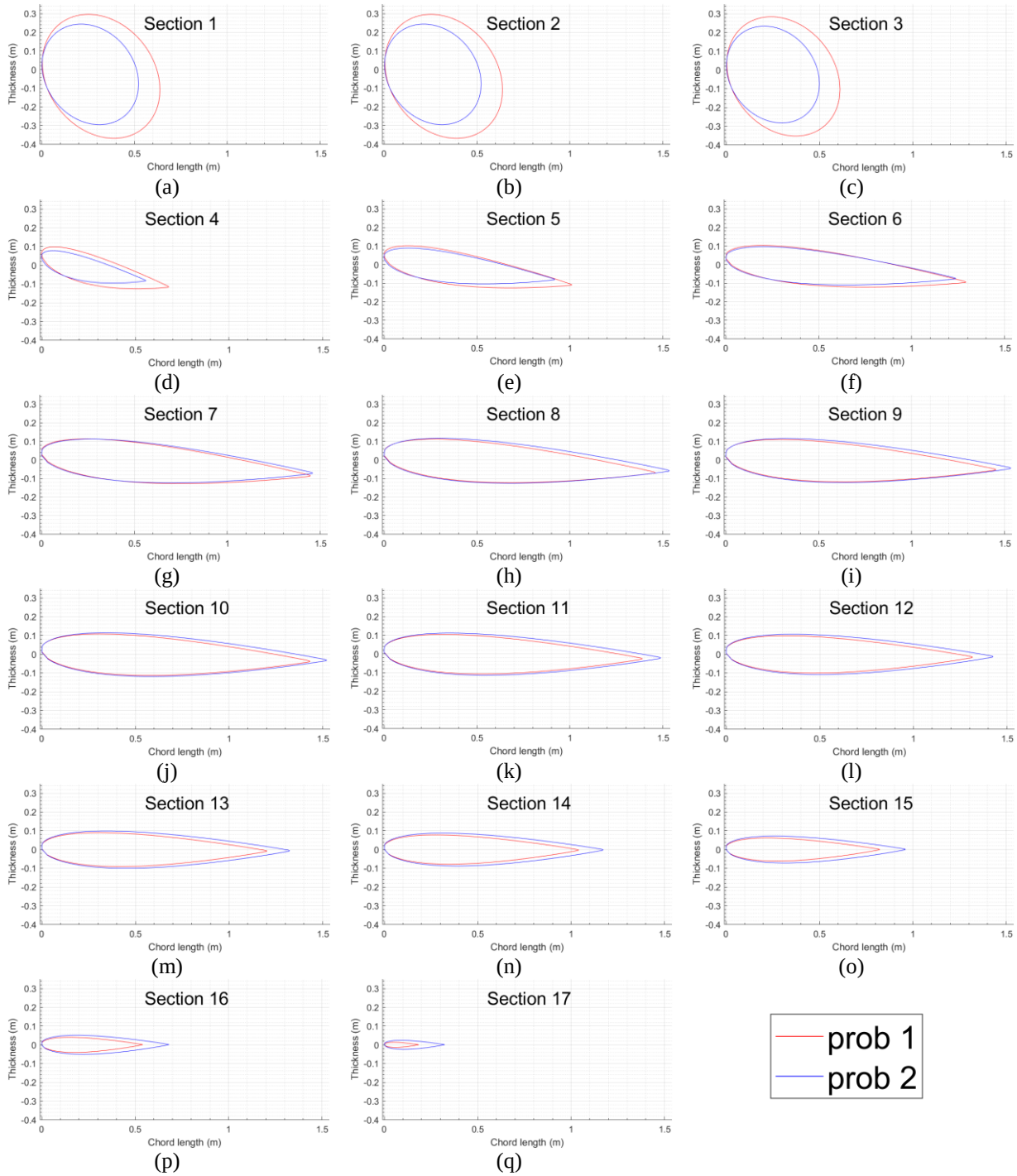

Fig. 6. Optimal design of airfoil in first and second problem (a) section 1, (b) section 2, (c) section 3, (d) section 4, (e) section 5, (f) section 6, (g) section 7, (h) section 8, (i) section 9, (j) section 10, (k) section 11, (l) section 12, (m) section 13, (n) section 14, (o) section 15, (p) section 16, (q) section 17.

Table 6: Real design variables from L-SHADE

	Problem 1				Problem 2			
Upper skins								
		Thickness		Orientation		Thickness		Orientation
Layer 1	$x_1 =$	0.0040 (m)	$x_6 =$	45 (deg)	$x_1 =$	0.0015 (m)	$x_6 =$	0 (deg)
Layer 2	$x_2 =$	0.0016 (m)	$x_7 =$	135 (deg)	$x_2 =$	0.0021 (m)	$x_7 =$	90 (deg)
Layer 3	$x_3 =$	0.0049 (m)	$x_8 =$	135 (deg)	$x_3 =$	0.0046 (m)	$x_8 =$	0 (deg)
Layer 4	$x_4 =$	0.0013 (m)	$x_9 =$	45 (deg)	$x_4 =$	0.0032 (m)	$x_9 =$	0 (deg)
Layer 5	$x_5 =$	0.0005 (m)	$x_{10} =$	135 (deg)	$x_5 =$	0.0027 (m)	$x_{10} =$	90 (deg)
Lower skins								
		Thickness		Orientation		Thickness		Orientation
Layer 1	$x_{11} =$	0.0008 (m)	$x_{16} =$	90 (deg)	$x_{11} =$	0.0019 (m)	$x_{16} =$	90 (deg)
Layer 2	$x_{12} =$	0.0002 (m)	$x_{17} =$	135 (deg)	$x_{12} =$	0.0001 (m)	$x_{17} =$	90 (deg)
Layer 3	$x_{13} =$	0.0009 (m)	$x_{18} =$	45 (deg)	$x_{13} =$	0.0007 (m)	$x_{18} =$	45 (deg)
Layer 4	$x_{14} =$	0.0006 (m)	$x_{19} =$	45 (deg)	$x_{14} =$	0.0002 (m)	$x_{19} =$	90 (deg)
Layer 5	$x_{15} =$	0.0003 (m)	$x_{20} =$	135 (deg)	$x_{15} =$	0.0012 (m)	$x_{20} =$	135 (deg)
Ribs								
		Thickness		Orientation		Thickness		Orientation
Layer 1	$x_{21} =$	0.001 (m)	$x_{26} =$	90 (deg)	$x_{21} =$	0.001 (m)	$x_{26} =$	45 (deg)
Layer 2	$x_{22} =$	0.001 (m)	$x_{27} =$	135 (deg)	$x_{22} =$	0.002 (m)	$x_{27} =$	135 (deg)
Layer 3	$x_{23} =$	0.001 (m)	$x_{28} =$	45 (deg)	$x_{23} =$	0.001 (m)	$x_{28} =$	0 (deg)
Layer 4	$x_{24} =$	0.001 (m)	$x_{29} =$	135 (deg)	$x_{24} =$	0.001 (m)	$x_{29} =$	90 (deg)
Layer 5	$x_{25} =$	0.002 (m)	$x_{30} =$	45 (deg)	$x_{25} =$	0.003 (m)	$x_{30} =$	0 (deg)
Spars								
		Thickness		Orientation		Thickness		Orientation
Layer 1	$x_{31} =$	0.0015 (m)	$x_{36} =$	90 (deg)	$x_{31} =$	0.0015 (m)	$x_{36} =$	135 (deg)
Layer 2	$x_{32} =$	0.0015 (m)	$x_{37} =$	90 (deg)	$x_{32} =$	0.0015 (m)	$x_{37} =$	90 (deg)
Layer 3	$x_{33} =$	0.0015 (m)	$x_{38} =$	135 (deg)	$x_{33} =$	0.0015 (m)	$x_{38} =$	45 (deg)
Layer 4	$x_{34} =$	0.0015 (m)	$x_{39} =$	90 (deg)	$x_{34} =$	0.0015 (m)	$x_{39} =$	90 (deg)
Layer 5	$x_{35} =$	0.0015 (m)	$x_{40} =$	90 (deg)	$x_{35} =$	0.0015 (m)	$x_{40} =$	135 (deg)
Chord distribution								
Control points	$x_{41} =$	0.6916	(m)		$x_{41} =$	0.5633	(m)	
	$x_{42} =$	4.0976	(m)		$x_{42} =$	4.4815	(m)	
	$x_{43} =$	1.4610	(m)		$x_{43} =$	1.5366	(m)	
	$x_{44} =$	0.1836	(m)		$x_{44} =$	0.3222	(m)	
Twist distribution								
Control points	$x_{45} =$	12.8346	(deg)		$x_{45} =$	11.1778	(deg)	
	$x_{46} =$	3.1618	(m)		$x_{46} =$	3.0254	(m)	
	$x_{47} =$	5.7585	(deg)		$x_{47} =$	5.0024	(deg)	
	$x_{48} =$	-0.1809	(deg)		$x_{48} =$	-0.1929	(deg)	
Mass of wind turbine blade								
		180.0153 (kg)				233.8253 (kg)		
Power of wind turbine								
		90.0018 (kW)				95.1360 (kW)		
Constraints								
	$g_1 =$	-0.0147			$g_1 =$	-0.0286		
	$g_2 =$	-0.0029			$g_2 =$	-0.0072		
	$g_3 =$	-0.0902			$g_3 =$	-0.0024		
	$g_4 =$	-1.8178						

5. Conclusions

In this study, the optimum designs of LS-WT in two different scenarios are obtained. The SOMHs illustrate the contrasting optimal solutions for different LS-WT problems, which have different objectives in problem definition. In the first problem, the mass of the WT is lower than in the second problem, aligning with the specified objective of minimizing mass. Conversely, the second problem prioritizes maximizing WT power and minimizing WT mass by weighted sum technique. This approach yields higher power output but results in a heavier design compared to the first problem. In the single-objective LS-WT problems, a comparative study of SOMHs was conducted over 10 runs, revealing that the L-SHADE algorithm emerged as the top performer. L-SHADE outperformed all competitors in both speed and consistency aspects. It is worth investigating the development of better variants of L-SHADE for solving WT optimization problems in future work.

Acknowledgements

This work was supported by the "Research Fund for Supporting Lecturer to Admit High Potential Student to Study and Research on His Expert Program Year 2019" scholarship, Graduated School, Khon Kaen University, Thailand, Grant No. 621T226. The authors are also grateful for the support from the National Research Council of Thailand (NRCT), Grant No. N42A650549

Declaration of Generative AI in Scientific Writing

The authors used ChatGPT for grammar corrections and readability improvement of the manuscript. Afterwards, the authors reviewed and edited the content and take full responsibility for the content of the publication.

References

[1] Arivalagan S, Sappani R, Čep R, Kumar MS. Optimization and experimental investigation of 3D printed micro wind turbine blade made of PLA material. Materials. 2023;16(6):2508.

[2] Amjith LR, Bavanish B. Optimization of horizontal axis wind turbine blade using FEA. Mater Today: Proc. 2021;37:3367-3371.

[3] Alkhabbaz A, Yang HS, Weerakoon AHS, Lee YH. A novel linearization approach of chord and twist angle distribution for 10 kW horizontal axis wind turbine. Renew Energy. 2021;178:1398-1420.

[4] Albanesi AE, Peralta I, Bre F, Storti BA, Fachinotti VD. An optimization method based on the evolutionary and topology approaches to reduce the mass of composite wind turbine blades. Struct Multidisc Optim. 2020;62:619-643.

[5] Castro O, Belloni F, Stolpe M, Yeniceli SC, Berring P, Branner K. Optimized method for multi-axial fatigue testing of wind turbine blades. Compos Struct. 2021;257:113358.

[6] Yang K. Geometry design optimization of a wind turbine blade considering effects on aerodynamic performance by linearization. Energies. 2020;13(9):2320.

[7] Rodriguez CV, Celis C. Design optimization methodology of small horizontal axis wind turbine blades using a hybrid CFD/BEM/GA approach. J Braz Soc Mech Sci Eng. 2022;44:254.

[8] Mitchell M. An introduction to genetic algorithms. Cambridge: MIT Press; 1998.

[9] Pourrajabian A, Dehghan M, Rahgozar S. Genetic algorithms for the design and optimization of horizontal axis wind turbine (HAWT) blades: a continuous approach or a binary one?. Sustain Energy Technol Assess. 2021;44:101022.

[10] Karaboga D. Artificial bee colony algorithm. Scholarpedia. 2010;5(3):6915.

[11] Zhu J, Cai X, Ma D, Zhang J, Ni X. Improved structural design of wind turbine blade based on topology and size optimization. Int J Low-Carbon Technol. 2022;17:69-79.

[12] Kennedy J, Eberhart R. Particle swarm optimization. Proceedings of ICNN'95 - International Conference on Neural Networks; 1995 Nov 27 - Dec 1; Perth, Australia. USA: IEEE; 1995. p. 1942-1948.

[13] Tanabe R, Fukunaga A. Evaluating the performance of SHADE on CEC 2013 benchmark problems. 2013 IEEE Congress on Evolutionary Computation; 2013 Jun 20-23; Cancun, Mexico. USA: IEEE; 2013. p. 1952-1959.

[14] Tanabe R, Fukunaga A. Success-history based parameter adaptation for differential evolution. 2013 IEEE Congress on Evolutionary Computation; 2013 Jun 20-23; Cancun, Mexico. USA: IEEE; 2013. p. 71-78.

[15] Tanabe R, Fukunaga AS. Improving the search performance of SHADE using linear population size reduction. 2014 IEEE Congress on Evolutionary Computation (CEC); 2014 Jul 6-11; Beijing, China. USA: IEEE; 2014. p. 1658-1665.
[16] Piotrowski AP. L-SHADE optimization algorithms with population-wide inertia. Inf Sci. 2018;468:117-141.
[17] The MathWorks Inc. Chinese Pangolin Optimizer (CPO) [Internet]. 2024 [cited 2024 Feb 24]. Available from: https://www.mathworks.com/matlabcentral/fileexchange/157086-chinese-pangolin-optimizer-cpo.
[18] Zhao W, Wang L, Zhang Z, Fan H, Zhang J, Mirjalili S, et al. Electric eel foraging optimization: a new bio-inspired optimizer for engineering applications. Expert Syst Appl. 2024;238:122200.
[19] Faramarzi A, Heidarinejad M, Mirjalili S, Gandomi AH. Marine Predators Algorithm: a nature-inspired metaheuristic. Expert Syst Appl. 2020;152:113377.
[20] Zhao W, Wang L, Zhang Z, Mirjalili S, Khodadadi N, Ge Q. Quadratic Interpolation Optimization (QIO): a new optimization algorithm based on generalized quadratic interpolation and its applications to real-world engineering problems. Comput Methods Appl Mech Eng. 2023;417:116446.
[21] Akbari V, Naghashzadegan M, Kouhikamali R, Afsharpanah F, Yaïci W. Multi-objective optimization and optimal airfoil blade selection for a small Horizontal-Axis Wind Turbine (HAWT) for application in regions with various wind potential. Machines. 2022;10(8):687.
[22] Yang S, Lee S, Yee K. Inverse design optimization framework via a two-step deep learning approach: application to a wind turbine airfoil. Eng Comput. 2023;39:2239-2255.
[23] Özkan R, Genç MS. Aerodynamic design and optimization of a small-scale wind turbine blade using a novel artificial bee colony algorithm based on blade element momentum (ABC-BEM) theory. Energy Convers Manage. 2023;283:116937.
[24] Ning A. Using blade element momentum methods with gradient-based design optimization. Struct Multidisc Optim. 2021;64:991-1014.
[25] Sagimbayev S, Kylyshbek Y, Batay S, Zhao Y, Fok S, Soo Lee T. 3D multidisciplinary automated design optimization toolbox for wind turbine blades. Processes. 2021;9(4):581.
[26] Yirtici O, Tuncer IH. Aerodynamic shape optimization of wind turbine blades for minimizing power production losses due to icing. Cold Reg Sci Technol. 2021;185:103250.
[27] Lee SL, Shin SJ. Structural design optimization of a wind turbine blade using the genetic algorithm. Eng Optim. 2022;54(12):2053-2070.
[28] Serafeim GP, Manolas DI, Riziotis VA, Chaviaropoulos PK, Saravanos DA. Optimized blade mass reduction of a 10MW-scale wind turbine via combined application of passive control techniques based on flap-edge and bend-twist coupling effects. J Wind Eng Ind Aerodyn. 2022;225:105002.
[29] Hayat K, Siddique S, Sultan T, Ali HT, Aloufi FA, Halawani RF. Effect of spar design optimization on the mass and cost of a large-scale composite wind turbine blade. Energies. 2022;15(15):5612.
[30] Wang Z, Suiker ASJ, Hofmeyer H, van Hooff T, Blocken B. Coupled aerostructural shape and topology optimization of horizontal-axis wind turbine rotor blades. Energy Convers Manage. 2020;212:112621.
[31] Thapa M, Missoum S. Surrogate-based stochastic optimization of horizontal-axis wind turbine composite blades. Struct Multidisc Optim. 2022;65:41.
[32] Belfkira Z, Mounir H, El Marjani A. Structural optimization of a horizontal axis wind turbine blade made from new hybrid composites with kenaf fibers. Compos Struct. 2021;260:113252.
[33] Özkan R, Genç MS. Multi-objective structural optimization of a wind turbine blade using NSGA-II algorithm and FSI. Aircr Eng Aerosp Technol. 2021;93(6):1029-1042.
[34] Yao S, Chetan M, Griffith DT, Escalera Mendoza AS, Selig MS, Martin D, et al. Aero-structural design and optimization of 50 MW wind turbine with over 250-m blades. Wind Eng. 2022;46(1):273-295.
[35] Al-Abadi A, Ertunç Ö, Beyer F, Delgado A. Torque-matched aerodynamic shape optimization of HAWT rotor. J Phys: Conf Ser. 2014;555:012003.
[36] Mahmuddin F. Rotor blade performance analysis with blade element momentum theory. Energy Procedia. 2017;105:1123-1129.
[37] El Khchine Y, Sriti M. Improved Blade Element Momentum theory (BEM) for predicting the aerodynamic performances of Horizontal Axis Wind Turbine Blade (HAWT). Technische Mechanik. 2018;38(2):191-202.
[38] Moriarty PJ, Hansen AC. AeroDyn theory manual. Technical report. USA: National Renewable Energy Lab; 2005. Report no.: NREL/TP-500-36881.
[39] University of Cambridge. Failure of laminates and the Tsai–Hill criterion [Internet]. 2023 [cited 2023 Nov 7]. Available from: https://www.doitpoms.ac.uk/tlplib/fibre_composites/laminate_failure.php.
[40] Cifuentes AO. Using MSC/NASTRAN: statics and dynamics. New York: Springer-Verlag; 2012.
[41] Leipholz H, Hutchinson JW. Theory of elasticity. J Appl Mech. 1975;42(4):911.

[42] Qiu Z, Li X. A new model for the eigenvalue buckling analysis with unknown-but-bounded parameters. Aerosp Sci Technol. 2021;113:106634.
[43] Hu W, Park D, Choi D. Structural optimization procedure of a composite wind turbine blade for reducing both material cost and blade weight. Eng Optim. 2013;45(2):1469-1487.
[44] Jureczko M, Mrówka M. Multiobjective optimization of composite wind turbine blade. Materials. 2022;15(13):4649.
[45] Wang R, Zhou Z, Ishibuchi H, Liao T, Zhang T. Localized weighted sum method for many-objective optimization. IEEE Trans Evol Comput. 2018;22(1):3-18.
[46] Storn R, Price K. Differential evolution – a simple and efficient heuristic for global optimization over continuous spaces. J Glob Optim. 1997;11:341-359.